# A novel theoretical study of elastic and electronic properties of $Os_2YAl$, (Y=Sc, Ti, V) Heusler Alloys

L. Taouaf[a,b], M. Mebrek[a,b], M. Sofiane Bendelhoum[b], and M. Berber[a,b,*]

[a]*Laboratoire d'Instrumentation et Matériaux Avancés,*
*Centre Universitaire Nour Bachir El-Bayadh, BP 900 route Aflou, 32000, Algeria.*
[b]*Centre Universitaire Nour Bachir El Bayadh, 32000 El Bayadh, Algeria.*
[*]*e-mail: berbermohamed@yahoo.fr*
*orcid: http://orcid.org/0000-0003-1285-3070*

Received 15 February 2022; accepted 8 March 2022

In this study, we have investigated the structural, electronic, and elastic properties of a new series of $Os_2YAl$, (Y=Sc, Ti, V) alloys called "Full Heusler", based on the Wien2k code using the functional density theory (DFT). The exchange and correlation energy are evaluated as part of the LDA approximation. The results showed that Os2VAl was more stable and harder than $Os_2ScAl$, and $Os_2TiAl$. The electronic band structures and density of states (DOS) of the compounds indicate that they are metallic because there is no bandgap in these three materials these results have been shown by three approaches (LDA, TB-mBJ, and SOC). Near the Fermi level, the energy is mainly occupied by the Os-5d and Sc, Ti, V-3d electrons. According to the results of the second-order elastic constants, these compounds met Born's criteria for mechanical stability. The elastic properties indicate that our compounds are ductile, anisotropic, and rigid. All the calculations and the data were compared with the results obtained with different methods in terms of its mechanical and electronic behavior, $Os_2VAl$ was found to have better physical properties than $Os_2ScAl$, and $Os_2TiAl$.

*Keywords:* Full-Heusler alloy; metallic; Ab-Initio calculations.

DOI: https://doi.org/10.31349/RevMexFis.68.061001

## 1. Introduction

Heusler alloys were discovered in 1903 by Fritz Heusler, they are gaining more and more attention from researchers [1]. Full and Half-Heusler alloys have a broad family of multifunctional materials for spintronic compound [2-8], shape memory alloys [9], superconducting ground state [10], and thermoelectric materials [11], Heusler alloys have Slater-Pauling behavior [12], higher curie temperature [13-15], Heusler's alloys are important materials in terms of their interesting properties such as electronic localization, itinerant magnetism, antiferromagnetism, helimagnetism, Pauli paramagnetism or the behavior of heavy fermions [16], Many researchers have discovered some full-Heusler alloys are not half-metals, but they present a metallic character because of the metallic nature of their spin-polarized electronic structures [17-20]. Among full-Heusler alloys, the Rh2CrGe [17] and Rh2MnTi alloys [18] which showed the metallic character, due to overlap between valence bands and conduction bands at the Fermi level with the two spins channels. While other researchers have shown that the metallic character of certain compounds products from the contribution of Rh, and (Cr,Mn)-3d states around the Fermi level [17,18]. The regular Heusler compounds $X_2YZ$, with 2:1:1 stoichiometry, crystallize in the cubic $L_{21}$ structure ($Fm3\bar{m}$, space group 225) with $Cu_2MnAl$ as the prototype [21,22]. Generally, the X and Y are transition metals and Z atoms are from III, IV, and V group elements [23]. If the atomic number Z(Y) $>$ Z(X), then the inverse Heusler structure XYXZ (prototype $Cu_2HgTi$, $F\bar{4}3m$, space group 216) is formed [21], or in the particular case when the Y element is more electronegative than X, the crystal structure observed for full-Heusler compounds, has $Cu_2$ HgTi prototype and $F\bar{4}3m$ space group [22]. The discovery of the giant magnetoresistance effect (GMR) in magnetic multilayer has revolutionized the field of information technology. Today, we are in contact with spintronics in our daily lives. Giant magnetoresistance (GMR) are used in magnetic hard drives, position detection on pneumatic cylinders, Position detection in robotics, speed measurement and position of ball bearings, wheel speed measurement, detection of banknotes by measurement of the magnetic ink, detection of electrical short circuits (*e.g*, in batteries), vehicle detection (road traffic count), and the Earth's magnetic field detection. The objective of this study is to predict the structural parameters, electronic structure, magnetic properties, and elastic properties of $Os_2YAl$, (Y=Sc, Ti, V) Heusler alloys by using the first-principles calculations of the full-potential (linearized) augmented plane wave (FP-(L)APW) method. This document is organized as follows: computational details are described in Sec. 2, the results are discussed in Sec. 3, and finally, the conclusions are presented in Sec. 4.

## 2. Calculation details

Electronic structure calculations of our full-Heusler compounds were performed using the first-principle calculations of density functional theory [24,25] based on the FP(L)APW method is implemented in the Wien2k code [26-29]. For

exchange-correlation potential, we used the local density approximation (LDA) proposed by Perdew and Wang [30], and the GGA-PBE approximation proposed by JP. Perdew, K. Burke, and M. Ernzerhof [31]. It calculates the self - consistent solution of the equations of Kohn and Sham [25]. In these calculations, we have chosen the values of the radii of the atoms of Os, Ti, Sc, V and Al of 2.2, 2, 2, 2.1 and 2 u.a, respectively, so that there is no overlap Muffin-Tin spheres. The electronic configurations of the sets of the system studied are: Os ($6s^2 4f^1 45d^3$), Ti ($3d^2\ 4s^2$), Sc ($3d^1\ 4s^2$), V ($3d^3\ 4s^2$), and Al ($3s^2\ 3p^1$). We have used a 1500K-point Monkhorst-Pack mesh [32,33] in the Brillouin zone for all compounds. We chose the $R_{MT} \times K_{\max} = 7$ (where $R_{MT}$ is the mean radius of muffin-tin spheres). The energy cutoff was chosen as $-6$ Ry, used for separation between the valence and the core states. The basic functions and potentials are extended in combinations of spherical harmonics around atomic sites, that is to say, the atomic spheres with a cutoff of $l_{\max} = 10$, and in Fourier series in the interstitial. The self-consistent convergence of the total energy was set at 0.1 mRy.

## 3. Results and discussion

### 3.1. Structural properties

The compounds $Os_2YAl$, (Y=Sc, Ti, and V), as most "Full Heusler" alloys crystallize in type structure "regular" ($Cu_2$ MnAl, $L_{21}$ prototype) with space group $Fm\bar{3}m$ N°:225, the atoms are located at the Wyckoff coordinates: with Os atoms are positioned at 8c (0.25,0.25,0.25), Y=Sc, Ti, V atoms at 4b (0.5,0.5,0.5), and Al 4a (0,0,0) [34]. The CrySDen [35] package has been used to plot the crystal structure of $Os_2YAl$, (Y=Ti, Sc, V), as shown in Fig. 1. We used Michael Gillisen's parameter with a magnetic moment equal to zero [36], and the data available [34,37] so we performed detailed structural optimizations by minimizing all energies. Figure 2 presents the total energy as a function of the volume for the three compounds. We have plotted the evolution of the total energy as a function of the volume according to the Murnaghan equation [38] given by the following relation,

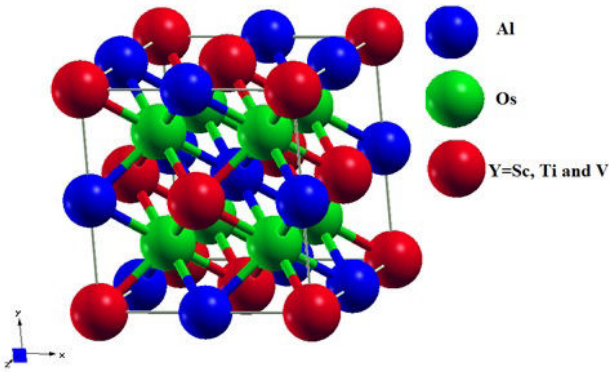


FIGURE 1. Crystal Structure of $Os_2YAl$ (Y=Sc, Ti, and V).

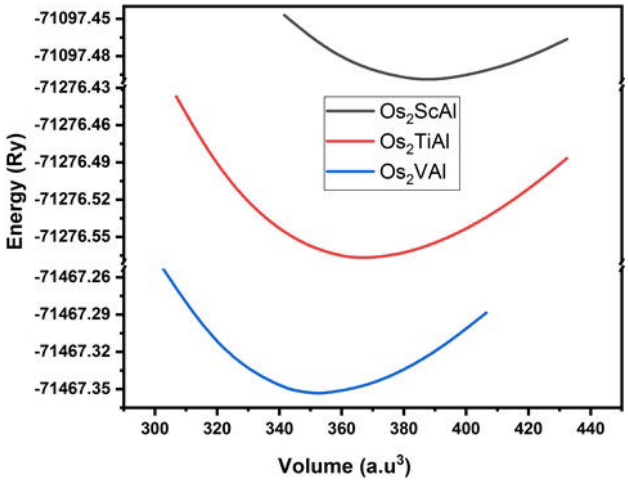


FIGURE 2. Total energy as a function of the volume of $Os_2YAl$ (Y=Sc, Ti, and V).

$$E = E_0 V + \frac{BV}{B(B-1)} \times \left( B\left[1 - \frac{V_0}{V}\right] + \left[\frac{V_0}{V}\right]^B - 1 \right), \quad (1)$$

where $E_0$ is the minimum energy at $T = 0$ K, B is the bulk modulus, B' is the bulk modulus derivative and $V_0$ is the equilibrium volume, all the points are effectuated by using the LDA approximation [30]. The optimized lattice parameter is almost the same as what has already been reported [34,36,37]. The results concerning the optimization of three materials $Os_2YAl$, (Y=Sc, Ti, V), (lattice parameters, the compressibility modulus, and their derivatives, and the equilibrium energies, optimized with the LDA and PBE), are grouped in Table I. The calculated lattice equilibrium constant values ($a_0$) of the $Os_2YAl$ compounds (y = Sc, Ti, and V) are compared to the lattice parameters available in the literature which are very close to each other [34,36,37]. The lattice constants for $Os_2ScAl$, $Os_2TiAl$, and $Os_2VAl$ differs by a percentage of approximately 1.83%, 1.8%, and 1.53%, respectively using LDA approximation, for PBE approach the results are improved. No experimental data were found for the lattice parameters of the compounds $Os_2TiAl$ and $Os_2VAl$ for comparison. The mass modulus calculated for the material $Os_2ScAl$ is closer to the available results [34]. For the mass modulus of the compounds $Os_2TiAl$ and $Os_2VAl$, no experimental value was found for comparison.

We can say that the $Os_2VAl$ compound has a higher negative energy and harder than $Os_2ScAl$, and $Os_2TiAl$ compounds due to the large value of the compressibility module. We note that when we go to an increased Sc-Ti-V and fixing X = Os and Z = Al, the mass modulus of $X_2YZ$ increases.

### 3.2. Formation and cohesive energy

To confirm the structural stability we calculated the cohesion energy and the energies of the individual atoms by increasing

TABLE I. Calculated equilibrium lattice constants $a$(Å), bulk modulus $B_0$ (GPa), and its first derivative $B'$, Equilibrium Energy, and the valence electron concentration (val-el), of $Os_2YAl$ (Y=Sc, Ti and V)

| | $a$(Å) | $B_0$ (GPa) | $B$' | $E_{Ch}$ (eV/atom) | $E_{\text{Fermi}}$ | E (Ry) | Method |
|---|---|---|---|---|---|---|---|
| Os2ScAl | 6.13 | 222.57 | 4.31 | -2.605 | 0.88 | -71097.499 | LDA |
| | 6.21 | 193.31 | 4.44 | | | -71152.061 | PBE |
| Previous [36] | 6.244 | | | | | | |
| | [34] | 6.268 | 194.26 | | | | |
| | [37] | 6.239 | | | | | |
| $Os_2TiAl$ | 6.01 | 273 | 4.24 | -2.614 | 0.92 | -71276.567 | LDA |
| | 6.09 | 233.82 | 4.84 | | | -71321.322 | PBE |
| Previous [36] | 6.12 | | | | | | |
| $Os_2VAl$ | 5.94 | 307.4 | 4.23 | -2.931 | 0.99 | -71467.353 | LDA |
| | 6.01 | 260.98 | 4.92 | | | -71512.273 | PBE |
| Previous [36] | 6.032 | | | | | | |

the unit cell of a face-centered cubic structure [39] up to 30 Bohr (about 16 Å) for the three compounds. The cohesion energy $E_{\text{coh}}^{Os_2yAl}$ of $Os_2YAl$ (Y=Si, Ti, V) is known as the overall energy of the constituent atoms minus the total energy of the compound is given by [39,40]

$$E_{\text{coh}}^{Os_2YAl} = \frac{E_{\text{Tot}}^{Os_2\,Y\,Al} - [xE_{\text{iso}}^{Os} + yE_{\text{iso}}^{Y} + zE_{\text{iso}}^{Al}]}{x+y+z}, \quad (2)$$

Y =Sc, Ti, and V with $E_{\text{iso}}^{Os}$, $E_{\text{iso}}^{Ti}$ $E_{\text{iso}}^{Al}$, refer to the energies of the isolated atoms, and $E_{\text{Tot}}^{Os_2\,Ti\,Al}$ is the total energy of the unit cell used in the present calculation, $x$, $y$, and $z$ are the numbers of atoms Os, Ti, Al in the unit cell respectively.

The cohesive energies are also indicated in Table I. It is found that the cohesion energy of the $Os_2ScAl$, $Os_2TiAl$ and $Os_2VAl$ compounds are $-2.605$ eV / atom, $-2.614$ eV/atom, and $-2.931$ eV/atom, respectively. From these results, we can say that the compound $Os_2VA$ has high stability compared to the compounds $Os_2ScAl$ and $Os_2TiAl$, and the $Os_2TiAl$ compound is more stable than the $Os_2ScAl$ compound. These results are comparable to the results of the optimization part.

### 3.3. Electronic properties

#### *3.3.1. Band structures*

Figures 3, 4 and 5, show the band structure of the studied systems $Os_2YAl$, (Y=Sc, Ti, V) with LDA, TB-mBJ [41-44], and LDA+SOC, respectively, calculated at their equilibrium lattice constants at different high points of symmetry in the Brillouin zone. The valence bands pass through the Fermi level and enter the conduction band for all structures, but do not overlap except $Os_2VAl$ for the three approximations, and the absence of a forbidden band which clearly indicates the metallic character. The dispersed upper bands are due to the strong hybridization of the (d) states of (Os, and Ti, Sc, and V). These results are similar to other results of the same family [34].

#### *3.3.2. Densities of states*

The projected total and partial state densities (DOST) (DOSP), between $-18.5$ and 9 are illustrated, respectively, in Figs. 4a), b), c), and the Fermi level is taken as the origin of the energies. The analysis of the figures of the total and partial state density of the $Os_2ScAl$, $Os_2TiAl$, and $Os_2VAl$ indicates a non-zero density at the Fermi level and the ab-

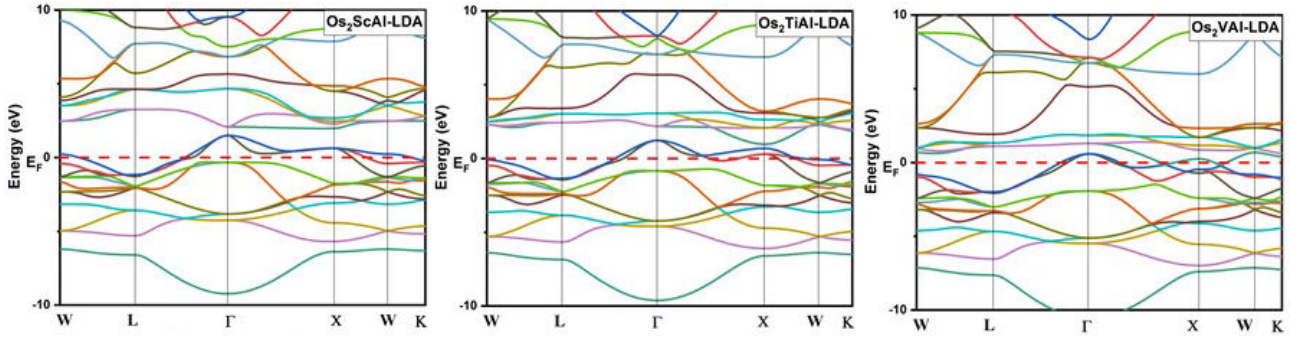


FIGURE 3. Band Structure of $Os_2YAl$ (Y=Sc, Ti, and V) with LDA approximation.

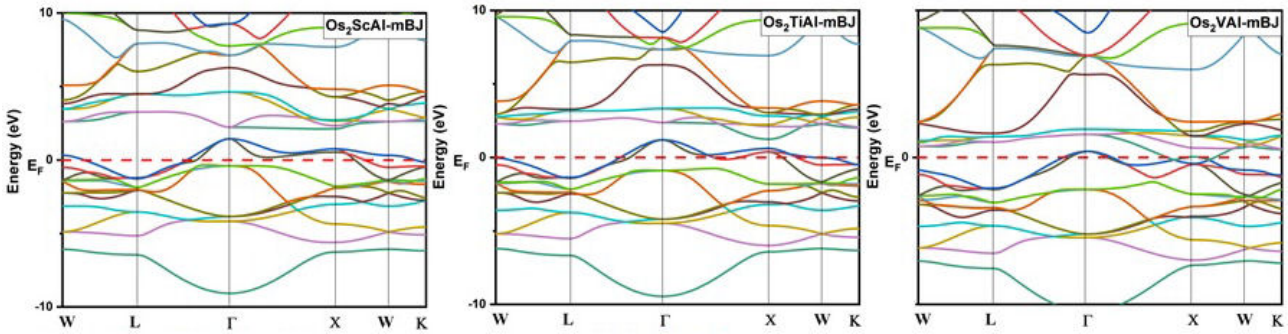


FIGURE 4. Band Structure of $Os_2YAl$ (Y=Sc, Ti, and V) with TB-mBJ approximation.

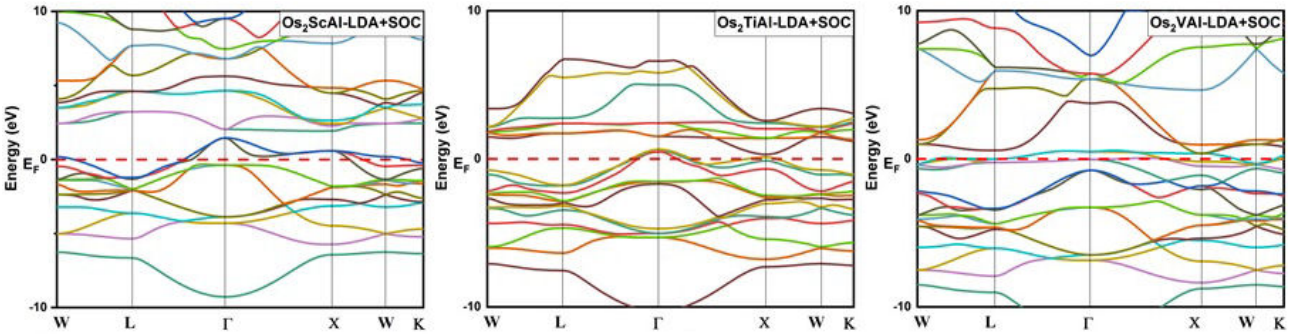


FIGURE 5. Band Structure of $Os_2YAl$ (Y=Sc, Ti, and V) with LDA+SOC approximation.

sence of the forbidden band $Eg$ which makes it possible to deduce that these materials have a metallic nature, (since the DOS has a great value at the Fermi level, see Table I). At the Fermi level, the DOS is 47.6, 34, and 13.6 states per cell unit per eV, respectively for $Os_2ScAl$, $Os_2TiAl$, and $Os_2VAl$. Therefore, there is a downward disposition concluded which makes $Os_2ScAl$ more conductive than $Os_2TiAl$ and $Os_2VAl$. We find that the TDOS around the Fermi level come mainly from electrons (Ti-d), and (Os-d) the states (p) of the (Al) elements occupy the lowest part of the valence states and have a small contribution around the Fermi level. In addition, there are two atoms of (Os), and only one atom of (Sc, Ti, and V) but the contribution of the Sc, Ti and V atoms is less efficient compared to the Os atom. The hybridization between the states Os (d), Y (d), and Al (p) becomes stronger when the lattice parameter increases with the atomic number of the elements (Y = Sc, Ti, and V). We can also see that the partial DOS of Y=Sc, Ti, and V (3d) orbitals in three materials exhibit the same behavior.

### 3.4. Elastic properties and mechanical stability

Furthermore, we have also considered to mechanical properties of the $Os_2YAl$ (Y=Sc, Ti, and V) full-Heusler alloy. The elastic properties describe the mechanical behavior of materials, their study is also important for the field of engineering. Knowledge of the elastic properties of materials is important for fundamental research, particularly for understanding the mechanisms of the bonds between atoms. The cubic structure materials have three independent elastic constants: $C_{11}$, $C_{12}$, and $C_{44}$. To obtain the elastic constants for these compounds, we used a first-principles numerical calculation using the method developed by Reshak and Morteza and integrated into the WIEN2k code [45]. From Table II, one can say that the $Os_2TiAl$, $Os_2ScAl$, and $Os_2VAl$ compounds are mechanically stable because all these elastic constants are positive and meet the criterion of mechanical stability verify the relation in Eq. (3) [46-49],

TABLE II. Elastic constant $C_{ij}$, and the anisotropic factors for the $Os_2YAl$ (Y=Sc, Ti and V).

| | $C_{11}$ (GPa) | $C_{12}$ (GPa) | $C_{44}$ (GPa) | A | $C_p = C_{12} - C_{44}$ |
|---|---|---|---|---|---|
| $Os_2ScAl$ | 308.73 | 181.67 | 98.73 | 1.55 | 82.94 |
| Previous [34] | 261.908 | 160.436 | 102.312 | 2.016 | 58.124 |
| $Os_2TiAl$ | 401.16 | 205.15 | 158.1 | 1.61 | 47.05 |
| $Os_2VAl$ | 516.9 | 202.98 | 163.6 | 1.04 | 39.38 |

TABLE III. The bulk modulus $B$, shear modulus $G$, Young's modulus $E$ Poisson's ratio $\nu$, and the bulk-modulus -to- shear-modulus ratio, for the $Os_2YAl$ (Y=Sc, Ti and V).

| | E(GPa) | B (GPa) | G (GPa) | $\nu$ | B/G |
|---|---|---|---|---|---|
| $Os_2ScAl$ | 220.99 | 224.02 | 82.735 | 0.32 | 2.70 |
| Previous [34] | 214.922 | 194.260 | 81.681 | 0.31 | 2.398 |
| $Os_2TiAl$ | 337.280 | 270.48 | 130.51 | 0.29 | 2.07 |
| $Os_2VAl$ | 411.04 | 307.61 | 160.9 | 0.27 | 1.90 |

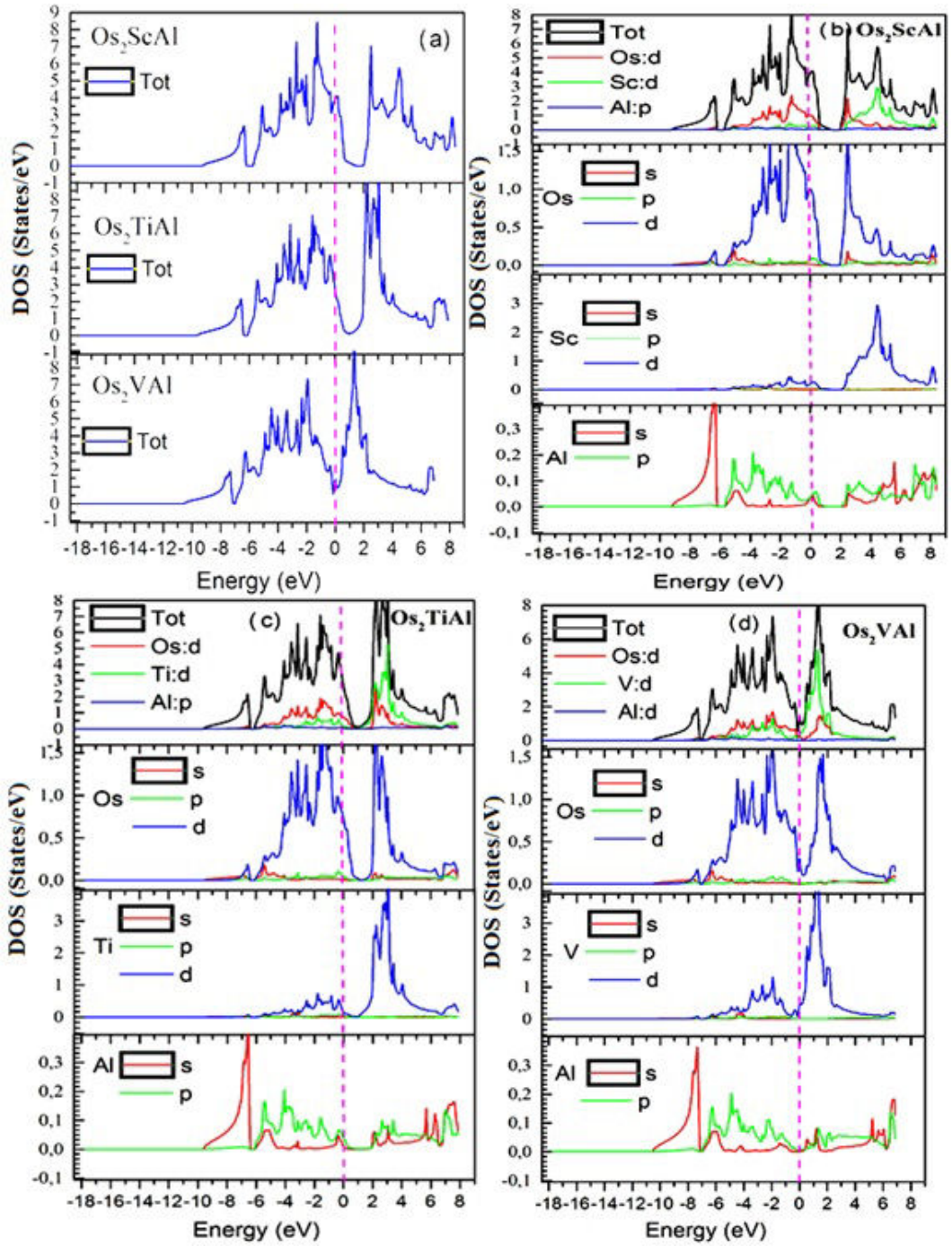


FIGURE 6. Total a) and partial density of states of $Os_2ScAl$ b), $Os_2TiAl$ c), $Os_2VAl$ d). The Fermi level is set to zero energy and marked by a vertical dashed line.

$$C_{11} > 0, \quad C_{44} > 0, \quad C_{11} - C_{12} > 0,$$
$$C_{11} + 2C_{12} > 0. \tag{3}$$

Our results show that the value of the $C_{11}$ constant is larger than the other constants for three compounds. So, we can say that the length change resistance is the most important in these compounds. The $C_{ij}$ modules have a heavyweight in the study of materials especially the $C_{44}$ module, from this module, can determine several properties such as fragility, among others. The $C_{44}$ module shows that $Os_2$VAl is harder than $Os_2$ TiAl, and $Os_2$ScAl; this result is similar to the one found in the optimization part. The elastic constants obtained for the compound $Os_2$ScAl are in good agreement with the available results, whereas the values of $C_{11}$ are greater than those reported in Ref. [34]. The value of $C_{44}$ was lower than the search result [34]. For the compounds $Os_2$TiAl, and $Os_2$VAl, no results were found for comparison. By comparing the $C_{11}$ values of the compounds studied, we verified that its values are of the increasing order according to the increase in the atomic number of the element Y = Sc, Ti, and V. According to Pettifor [50,51], the character of atomic bonding in metals and compounds, also relates to the brittle or ductile characteristics can be found by considering the Cauchy pressure (CP). A negative value of CP shows a strong covalent bond while a positive value of CP indicates a strong metallic bond. The Cauchy pressure values are 82.94 GPa, 47.05 GPa, and 39.38 GPa for $Os_2$ScAl, $Os_2$TiAl, and $Os_2$Val, respectively. The obtained values for the pressure are all positive, showing a metallic character and ductile nature of the compounds. These results confirm the metallic bonding character of the three materials, and the most stable compound was $Os_2$VA1, in agreement with the optimization and cohesive energy calculations, as well as the electronic band structure analysis.

The knowledge of the elastic constants $C_{ij}$ allows us to calculate other mechanical (elastic) quantities such as the modulus of compressibility $B$, the Young and shear modulus ($Y$ and $G$), as well as the Poisson's ratio ($\nu$) which are important parameters in technological applications and provide a fundamental description of the mechanical behavior of a material. The bulk modulus is used to measure the hardness of materials to volume variation by the applied hydrostatic pressure [47,48], while the shear modulus $G$ represents the resistance to plastic deformation and gives the behavior of a material under a uniform pressure [47-49]. For a cubic crystal the bulk modulus $B$, the Voight-Reuss-Hill averaged shear modulus $G$, Poisson's ratio $v$, and Young's modulus are expressed as follows [35,36,38,46-48,52-54].

$$B_V = B_R = \frac{(C_{11} + 2C_{12})}{3}, \tag{4}$$

$$G_V = \frac{(C_{11} - C_{12} + 3C_{44})}{5}. \tag{5}$$

The Reuss bounds [46,55] of the bulk and shear modulus are $B_V = B_R$ and

$$G_R = \frac{2C_{11}(C_{12} - 2C_{44})}{[4C_{44} + 3(C_{11} - 2C_{12})]}. \tag{6}$$

According to the Hill approximation [46,56] method, arithmetic mean of the Voigt and Reuss's shear moduli gives the elastic modulus expressed as following:

$$G = \frac{(G_V + G_R)}{2} = G_H, \tag{7}$$

where $G_V$ is the Voigt shear modulus and $G_R$ is the Reuss shear modulus.

The mass modulus ($B$) is greater than the shear modulus ($G$) for all three compounds. Thus, these materials must be resistant to changes in their volumes under uniform pressure. The results of the modulus of mass $B$ obtained as a function of the elastic constants are of the same order as the results obtained by applying the Murnaghan equation [38], displaying that our estimated results of the elastic constants for $Os_2$ScAl, $Os_2$TiAl, and $Os_2$VAl are exact and precise. The Young's modulus $E$ and Poisson's ratio $\nu$ for a cubic structure are related to the modulus of compressibility $B$ and shear $G$. Using the relation [36,46-48],

TABLE IV. Calculated total and local magnetic moments per atom unit cell (in units of the Bohr magneton $\mu$B), and in the interstitial sites for $Os_2$YAl, Y = Sc, Ti, and V.

| | $Os_2$ScAl | $Os_2$TiAl | $Os_2$VAl |
|---|---|---|---|
| $\mu^{Os}$ | 0.00089 | 0.00086 | 0.00026 |
| $\mu^{Sc}$ | 0.00145 | - | - |
| $\mu^{Ti}$ | - | 0.00141 | - |
| $\mu^{V}$ | - | - | 0.00005 |
| $\mu^{Al}$ | 0.00053 | 0.00001 | 0.00113 |
| $\mu^{inter}$ | 0.00311 | 0.00060 | 0.00040 |
| $\mu^{Total}$ | 0.00069, 0 [36] | 0.00028, 0 [36] | 0.00106, 0 [36] |

$$E = \frac{9BG}{(3B+G)}, \tag{8}$$

$$\nu = \frac{(3B-2G)}{2(3B+G)}. \tag{9}$$

The Young's modulus is defined as the ratio between stress and strain and is used to provide a measure of the stiffness of the solid matter, *i.e.*, the larger the value of $E$, entails a stiffer material [46,57]. We can see from the results mentioned in Table III, that the Young's modulus value $E$ is in ascending order, and $Os_2$VAl compound is more rigid and harder than $Os_2$ScAl and, $Os_2$TiAl due to its higher value of Young's modulus, and compressibility modulus ($B$). At the same time, the value of $E$ of compound $Os_2$ScAl is of the same order of results available [34].

With an increase in Poisson's ratio, the plasticity of the crystal improves. The Poisson's ratio has been suggested as 0.1 for covalent substances and 0.25 for ionic substances in the literature [17,58]. The Poisson ratios for the alloys $Os_2$ScAl, $Os_2$TiAl, and $Os_2$VAl are, respectively, 0.32, 0.29, and 0.27, (see Table III) which means that the alloys have a metallic ionic reaction. For an isotopic crystal $A = (2C_{44})/(C_{11} - C_{12})$ is equal to 1, but when there is another value greater or less than 1 it means that it is an anisotropic crystal [59,60]. According to Table II, the anisotropy coefficient exceeded unity, which indicates that our compounds have an anisotropic character. The Pugh criterion [59,61], is the ratio between the compressibility modulus and the shear modulus ($B/G$) of the polycrystalline phases could also be used as a measure to quantify whether a material breaks in a ductile or brittle manner. Subsequently, a high (low) value of this ratio is associated with ductility (brittleness). The critical value separating the ductile and the brittle turned out to be 1.75. As shown in Table III, this ratio is greater than 1.75 for the three $Os_2$ScAl, $Os_2$TiAl, and $Os_2$VAl compounds, which are classified as ductile compounds, and this result confirmed previous data [34].

## 4. Conclusion

In summary, we have studied the structural, elastic, and electronic properties of the Heusler $Os_2$YAl,(Y=Sc, Ti, V) alloy, with the space group $Fm\bar{3}m$ (# 225) in phase $L2_1$, which were calculated using first-principle calculations of the full-potential linearized augmented plane wave (FP-LAPW) method, with local density approximation. After fitting the Murnaghan equation of state, the equilibrium lattice parameters obtained from our calculation agree well with the theoretical values available. We found that the compound $Os_2$VAl is more stable and harder than $Os_2$ScAl, and $Os_2$TiAl, a result that was confirmed by the calculation of the cohesion energy. The calculated state densities presented in this study identify the metallic behavior of $Os_2$YAl, (Y=Sc, Ti, and V), by three approaches (LAD, mBJ, SOC). The metal band property of these compounds was confirmed based on the Cauchy pressure values. The elastic constants of these compounds are calculated according to the method developed by Reshak and Morteza and the results obtained show the compounds studied are mechanically stable. The Poisson's ratio values showed that the compounds had an ionic metallic character. Analysis of Young's modulus and the $B/G$ ratio shows that the three materials were rigid and ductile.


1. J. Duan, W. Yin-Wei, Z. A-Peng, S. Liu, and S. A. Dar, Electronic structure, elastic, mechanical, thermodynamic and thermoelectric investigations of $Mn_2PtX$ (X=Rh, Pd) Heusler alloys, *Solid State Commun.* **290** (2019) 12, https://doi.org/10.1016/j.ssc.2018.12.013.
2. S. Wurmehl, G. H. Fecher, H. C. Kandpal, V. Ksenofontov, and C. Felser, Investigation of $Co_2FeSi$: The Heusler compound with highest Curie temperature and magnetic moment, *Appl. Phys. Lett.* **88** (2006) 032503, https://doi.org/10.1063/1.2166205.
3. Y, Miura, K. Nagao, and M. Shirai, Atomic disorder effects on half-metallicity of the full-Heusler alloys $Co_2(Cr_{1-x}Fe_x)Al$: A first-principles study, *Phys. Rev. B* **69** (2004) 144413,
4. H. Ohno, Properties of ferromagnetic III-V semiconductors, *J. Magn. Magn. Mater.* **200** (1999) 110, https://doi.org/10.1016/S0304-8853(99)00444-8.
5. R. A. de Groot, F. M. Mueller, P. G. van Engen, and K. H. J. Buschow, New Class of Materials: Half-Metallic Ferromagnets, *Phys. Rev. Lett.* **50** (1983) 2024, https://doi.org/10.1103/PhysRevLett.50.2024.
6. S. A. Wolf et al., Spintronics: A Spin-Based Electronics Vision for the Future, *Science* **294** (2001) 1488, https://doi.org/10.1126/science.1065389.
7. S. J. Hashemifar, P. Kratzer, and M. Scheffler, Preserving the Half-Metallicity at the Heusler Alloy $Co_2MnSi(001)$ Surface: A Density Functional Theory Study, *Phys. Rev. Lett.* **94** (2005) 096402, https://doi.org/10.1103/PhysRevLett.94.096402.
8. F. Aguilera-Granja, R. H. Aguilera-del-Toro and J. L. Morán-López, *Mater. Res. Express* **6** (2019) 106118.
9. F. Aguilera-Granja, R. H. Aguilera-del-Toro and J. L. Morán-López, A first principles systematic study of the structural, electronic, and magnetic properties of Heusler $X_2MnZ$ with X=Fe, Co, Ni, Cu, Ru, Rh, Pd, Ag, Pt, Au and Z = Al, Si, Ga, Ge, In and Sn, *Mater. Res. Express* **6** (2019) 106118, https://doi.org/10.1088/2053-1591/ab243c.
10. R. Kainuma *et al.*, Magnetic-field-induced shape recovery by reverse phase transformation, *Nature* **439** (2006) 957, https://doi.org/10.1038/nature04493.
11. J.-W. G. Bos and R. A. Downie, Half-Heusler thermo-

electrics: a complex class of materials, *J. Phys. Condens. Matter* **26** (2014) 433201, https://doi.org/10.1088/0953-8984/26/43/433201.

12. I. Galanakis, P. H. Dederichs, and N. Papanikolaou, Slater-Pauling behavior and origin of the half-metallicity of the full-Heusler alloys, *Phys. Rev. B* **66** (2002) 174429, https://doi.org/10.1103/PhysRevB.66.174429.

13. S. Amari, R. Mebsout, S. Méçabih, B. Abbar, and B. Bouhafs, First-principle study of magnetic, elastic and thermal properties of full Heusler $Co_2MnSi$, *Intermetallics* **44** (2014) 26, https://doi.org/10.1016/j.intermet.2013.08.009.

14. S. Maier et al., Order-disorder transitions in the $Fe_2Val$ Heusler alloy, *Acta Mater.* **121** (2016) 126, https://doi.org/10.1016/j.actamat.2016.08.080.

15. A. Bentouaf and F. E. H. Hassan, Structural, electronic, magnetic and thermodynamic properties of full-Heusler compound $Co_2VSi$: Ab initio study, *J. Magn. Magn. Mater.* **381** (2015) 65, https://doi.org/10.1016/j.jmmm.2014.12.065.

16. M. Zemouli *et al*., First-Principles Investigation of Elastic, Electronic, and Half-Metallic Ferrimagnetic Properties in the $Mn_2RhSi$ Heusler Alloy, *J. Supercond. Nov. Magn.* **29** (2016) 3187, https://doi.org/10.1007/s10948-016-3719-4.

17. S. Al, N. Arikan, S. Demir, and A. IyigÃ¶r, Lattice Dynamic properties of $Rh_2XAl$ (X=Fe and Y) alloys, *Phys. B* **531** (2018) 16, https://doi.org/10.1016/j.physb.2017.12.020.

18. S. Berri et al., Study of structural, electronic and magnetic properties of $Rh_2MnX$ (X=Al, Ge and Sn) Heusler alloys using GGA-WC and GGA+U approaches, *Phys. B* **418** (2013) 58,

19. F. Benzoudji, The Preference of the Ferromagnetic Ordering for the Novel Heusler $Rh_2MnTi$ Compound, *J. Supercond. Nov. Magn.* **32** (2019) 1415, https://doi.org/10.1007/s10948-018-4837-y.

20. M. Mebrek et al., Theoretical Investigation of Electronic Structures, Elastic, and Magnetic Properties of $Rh_2CrGe$ Full-Heusler Alloy, *Acta Phys. Pol. A* **136** (2019) 454, https://doi.org/10.12693/APhysPolA.136.454.

21. V. Alijani, J. Winterlik, G. H. Fecher, and C. Felser, Tuning the magnetism of the Heusler alloys $Mn_{3-x}Co_xGa$ from soft and half-metallic to hardmagnetic for spin-transfer torque applications, *Appl. Phys. Lett*. **99** (2011) 222510, https://doi.org/10.1063/1.3665260.

22. A. Birsan and P. Palade, Band structure calculation of $Ti_2FeSn$: A new half-metallic compound, *Intermetallics* **36** (2013) 86, https://doi.org/10.1016/j.intermet.2013.01.005.

23. D. P. Rai, S. Sandeep, M. P. Ghimire, and R. K. Thapa, Study of energy bands and magnetic properties of $Co_2CrSi$ Heusler alloy, *Bull. Mater. Sci.* **34** (2011) 1219, https://doi.org/10.1007/s12034-011-0233-y.

24. P. Hohenberg and W. Kohn, Inhomogeneous Electron Gas, *Phys. Rev.* **136** (1964) B864, https://doi.org/10.1103/PhysRev.136.B864.

25. K. Kohn and L. J. Sham, Self-Consistent Equations Including Exchange and Correlation Effects, *Phys. Rev.* **140** (1965) A1133, https://doi.org/10.1103/PhysRev.140.A1133.

26. P. Blaha *et al*., WIEN2k: *An Augmented Plane Wave + Local Orbitals Program for Calculating Crystal Properties*, Vienna, Austria.

27. P. Blaha et al., WIEN2k: An APW+lo program for calculating the properties of solids, *J. Chem. Phys.* **152** (2020) 074101, https://doi.org/10.1063/1.5143061.

28. K. Schwarz, DFT calculations of solids with LAPW and WIEN2k, *J. Solid State Chem.* **176** (2003) 319, https://doi.org/10.1016/S0022-4596(03)00213-5.

29. K. Schwarz, P. Blaha, and G. K. H. Madsen, Electronic structure calculations of solids using the WIEN2k package for material sciences, *Comput. Phys. Commun.* **147** (2002) 71, https://doi.org/10.1016/S0010-4655(02)00206-0.

30. J. P. Perdew and Y. Wang, Accurate and simple analytic representation of the electron-gas correlation energy, *Phys. Rev. B* **45** (1992) 13244, https://doi.org/10.1103/PhysRevB.45.13244.

31. J. P. Perdew, K. Burke, M. Ernzerhof, Generalized Gradient Approximation Made Simple, *Phys. Rev. Lett.* **7** (1996) 3865, https://doi.org/10.1103/PhysRevLett.77.3865.

32. H. J. Monkhorst and J. D. Pack, Special points for Brillouin-zone integrations, *Phys. Rev. B* **13** (1976) 5188, https://doi.org/10.1103/PhysRevB.13.5188.

33. J. D. Pack and H. J. Monkhorst, Special points for Brillouin-zone integrations-a reply, *Phys. Rev. B* **16** (1977) 1748, https://doi.org/10.1103/PhysRevB.16.1748.

34. N. Arikan, H. Y. Ocak, G. D. Yıldız, Y. G. Yıldız, and R. Ünal, Investigation of the Mechanical, Electronic and Phonon Properties of $X_2ScAl$ (X=Ir, Os, and Pt) Heusler Compounds, *J. Korean Phys. Soc*. **76** (2020) 916, https://doi.org/10.3938/jkps.76.916.

35. A. Kokalj, Computer graphics and graphical user interfaces as tools in simulations of matter at the atomic scale, *Comput. Mater. Sci.* **28** (2003) 155, https://doi.org/10.1016/S0927-0256(03)00104-6.

36. M. Gilleßen, Ph.D. thesis, RWTH Aachen University, 2009.

37. J. E. Saal, S. Kirklin, M. Aykol, B. Meredig, and C. Wolverton, Materials Design and Discovery with High-Throughput Density Functional Theory: The Open Quantum Materials Database (OQMD), *JOM* **65** (2013) 1501, https://doi.org/10.1007/s11837-013-0755-4.

38. F. D. Murnaghan, The Compressibility of Media Under Extreme Pressures, *Proc. Natl. Acad. Sci. U.S.A.* **30** (1944) 244, https://doi.org/10.1073/pnas.30.9.244.

39. M. Mebrek, A. Mokaddem, B. Doumi, A. Yakoubi, and A. Mir, A Novel Theoretical Study of Elastic and Electronic Properties of $M_2CdC$ (M=Zr, Hf, and Ta) MAX Phases, *Acta Phys. Pol. A* **133** (2017) 76, https://doi.org/10.12693/APhysPolA.133.76.

40. Z. W. Huang, Y. H. Zhao, H. Hou, and P. D. Han, Electronic structural, elastic properties and thermodynamics of $Mg_{17}Al_{12}$,

$Mg_2Si$, and $Al_2Y$ phases from first-principles calculations, *Phys. B* **407** (2012) 1075, https://doi.org/10.1016/j.physb.2011.12.132.

41. F. Tran, P. Blaha, and K. Schwarz, Band gap calculations with Becke- Johnson exchange potential, *J. Phys. Condens. Matter* **19** (2007) 196208, https://doi.org/10.1088/0953-8984/19/19/196208.

42. D. Koller, F. Tran, and P. Blaha, Improving the modified Becke-Johnson exchange potential, *Phys. Rev. B* **85** (2012) 155109, https://doi.org/10.1103/PhysRevB.85.155109.

43. D. Koller, F. Tran, and P. Blaha, Merits and limits of the modified Becke- Johnson exchange potential, *Phys. Rev. B* **83** (2011) 195134, https://doi.org/10.1103/PhysRevB.83.195134.

44. F. Tran and P. Blaha, Accurate Band Gaps of Semiconductors and Insulators with a Semilocal Exchange-Correlation Potential, *Phys. Rev. Lett.* **102** (2009) 226401, https://doi.org/10.1103/PhysRevLett.102.226401.

45. A. H. Reshak and M. Jamal, DFT Calculation for Elastic Constants of Tetragonal Structure of Crystalline Solids with WIEN2k Code: A New Package (Tetra-elastic), *Int. J. Electrochem. Sci.* **8** (2013) 12252.

46. M. L. Ali and M. Z. Rahaman, Investigation of different physical aspects such as structural, mechanical, optical properties and Debye temperature of $Fe_2ScM$ (M=P and As) semiconductors: A DFT-based first principles study, *Int. J. Mod. Phys. B* **32** (2018) 1850121, https://doi.org/10.1142/S0217979218501217.

47. F. Z. Benkhelifa, A. Lekhal, and S. Méçabih, GGA and GGA+$U$ Description of Structural, Magnetic, and Elastic Properties of $Rh_2MnZ$ (Z=Ge, Sn, and Pb), *J. Supercond. Nov. Magn.* **26** (2013) 2573, https://doi.org/10.1007/s10948-012-1815-7.

48. S. Qi, C.-H. Zhang, B. Chen, and J. Shen, First-principles study on the band structure, magnetic and elastic properties of half-metallic $Cr_2MnAl$, *Mod. Phys. Lett. B* **29** (2015) 1550139, https://doi.org/10.1142/S0217984915501390.

49. J. Wang, S. Yip, S. R. Phillpot, and D. Wolf, Crystal instabilities at finite strain, *Phys. Rev. Lett.* **71** (1993) 4182, https://doi.org/10.1103/PhysRevLett.71.4182.

50. D. G. Pettifor, Theoretical predictions of structure and related properties of intermetallics, *Mater. Sci. Technol.* **8** (1992) 345, https://doi.org/10.1179/mst.1992.8.4.345.

51. A. Abada, K. Amara, S. Hiadsi, and B. Amrani, First principles study of a new half-metallic ferrimagnets $Mn_2$-based full Heusler compounds: $Mn_2ZrSi$ and $Mn_2ZrGe$, *J. Magn. Magn. Mater.* **388** (2015) 59, https://doi.org/10.1016/j.jmmm.2015.04.023.

52. F. Ahmadian and R. Alinajimi, First-principles study of half-metallic properties for the Heusler alloys $Sc_2CrZ$ (Z=C,Si,Ge,Sn), *Comput. Mater. Sci.* **79** (2013) 345, https://doi.org/10.1016/j.commatsci.2013.06.034.

53. O. Cheref et al., First-principles study of half-metallic properties in $X_2VSi$ ($X$=Ti, Co) and their quaternaty TiCoVSi and CoTiVSi compounds, *Comput. Condens. Matter* **19** (2019) e00369, https://doi.org/10.1016/j.cocom.2019.e00369.

54. O. Canko, F. Taskin, M. Atis, N. Kervan, and S. Kervan, Magnetism and Half-Metallicity in the $Fe_2ZrP$ Heusler Alloy, *J. Supercond. Nov. Magn.* **29** (2016) 2573, https://doi.org/10.1007/s10948-016-3576-1.

55. A. Reuss, Berechnung der Fließgrenze von Mischkristallen auf Grund der Plastizitätsbedingung für Einkristalle, *Z. Angew. Math. Mech.* **9** (1929) 49, https://doi.org/10.1002/zamm.19290090104.

56. R. Hill, The Elastic Behaviour of a Crystalline Aggregate, *Proc. Phys. Soc. A* **65** (1952) 349, https://doi.org/10.1088/0370-1298/65/5/307.

57. S. Huang, R.-Z. Li, S.-T. Qi, B. Chen, and J. Shen, A theoretical study of the elastic and thermal properties of ScRu compound under pressure, *Phys. Scr.* **89** (2014) 065702, https://doi.org/10.1088/0031-8949/89/6/065702.

58. V. V. Bannikov, I. R. Shein, and A. L. Ivanovskii, Electronic structure, chemical bonding and elastic properties of the first thorium-containing nitride perovskite $TaThN_3$, *Phys. Status Solidi Rapid Res. Lett.* **1** (2007) 89, https://doi.org/10.1002/pssr.200600116.

59. S. Boucetta, Theoretical study of elastic, mechanical and thermodynamic properties of MgRh intermetallic compound, *J. Magn. Alloys* **2** (2014) 59, https://doi.org/10.1016/j.jma.2014.04.001.

60. C. Zener, Elasticity and Anelasticity of Metals (University of Chicago Press, Chicago, 1948).

61. S. F. Pugh, Relations between the elastic moduli and the plastic properties of polycrystalline pure metals, London Edinburgh Dublin Philos. *Mag. J. Sci*. **45** (1954) 823, https://doi.org/10.1080/14786440808520496.